

## LORENTZ FORCE INDUCED FLOW IN A CYLINDRICAL CONTAINER

*M.D. Marín-Núñez*<sup>1</sup>, *D.R. Domínguez-Lozoya*<sup>1,2</sup>,  
*E. Ramos*<sup>1</sup>, *S. Cuevas*<sup>1\*</sup>, *A. Beltrán*<sup>3</sup>

<sup>1</sup> *Instituto de Energías Renovables, Universidad Nacional Autónoma de México,  
62580 Temixco, Mor. Mexico*

*\*e-Mail: scg@ier.unam.mx*

<sup>2</sup> *Facultad de Ciencias Físico-Matemáticas, Universidad Autónoma de Sinaloa,  
80010 Culiacán, Sin. Mexico*

<sup>3</sup> *Instituto de Investigaciones en Materiales, Unidad Morelia,  
Universidad Nacional Autónoma de México, 58190 Morelia, Mich. Mexico*

An experimental electrolyte flow inside a cylindrical cavity promoted by a Lorentz force created by external electric currents and a magnetic field applied in the axial direction is discussed. The Lorentz force produces an azimuthal swirling flow that gives rise to a secondary poloidal flow. Supported by numerical simulations we found that a three-dimensional flow can be interpreted as being partially composed by toroidal orbits. The flows studied have common features with electrovortex flows, and it is expected that this study can contribute to their understanding.

### Introduction.

Flows within liquid metal batteries (LMB) are known to be critical to the performance, durability, and malfunction of these energy storage devices. Although the motion of the battery's liquid components is extremely complex, for purposes of analysis, simplified experiments can yield valuable insights, even if they do not fully replicate real operating conditions. In their review of the fluid dynamics of LMB, Kelly and Weier [1] indicate that relevant fluid dynamics phenomena in LMBs include thermal convection, magnetoconvection, Marangoni flow, interface instabilities, the Tayler instability, and electrovortex flow (EVF). The EVF is the motion driven by the interaction of an imposed or spontaneous electric current with its own induced magnetic field [2]. A key feature of this flow is that the Lorentz force induces a swirling motion, which, in turn, generates a boundary layer near rigid walls that are not parallel to the rotation axis. Convergent flow from these boundary layers results in a pumping flow that drives a secondary poloidal flow. Recent experiments and numerical simulations of liquid metal flows in the presence of an electric current have demonstrated that beyond a threshold azimuthal driving force, a transient poloidal EVF evolves. This motion slowly decays to be totally suppressed at long times [3]. The secondary flow may be of importance in the performance and stability of LMBs, specially in the transient state when batteries are switched on.

In this paper, we report an experimental and numerical study of a flow that reproduces some patterns that resemble structures found in EVF. We propose a flow model that has several similarities with electrovortex, but also differences that render advantages that permit a far simpler experimental exploration.

### 1. Experimental setup.

The main component of the experimental equipment is a glass cylindrical container, 0.015m and 0.03m in radius and height, respectively, filled with an aqueous

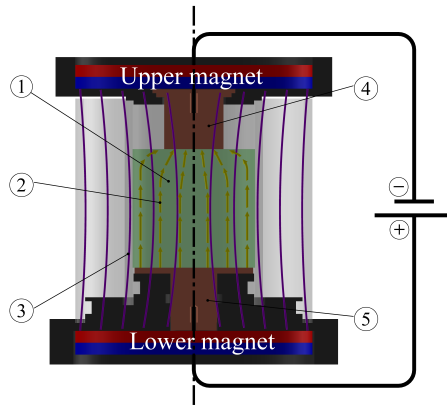


*Fig. 1.* Sketch of the experimental device showing the position of the electrodes and Neodymium magnets that generate an approximately uniform magnetic field. PIV was used to record the velocity field in a vertical plane containing the axis of symmetry. The plus sign (+) preceding the electric current quoted in the text indicates the power source polarity shown in the figure. (1) – cylindrical cell containing the electrolyte, (2) – electrical current lines, (3) – magnetic field lines, (4) – upper electrode, (5) – lower electrode.

solution of  $\text{NaHCO}_3$ , whose mass density, electrical conductivity and dynamic viscosity are  $\rho = 1.09 \times 10^3 \text{ kg/m}^3$ ,  $\sigma = 5.6 \text{ S/m}$  and  $\mu = 1.09 \times 10^{-3} \text{ kg/(m}\cdot\text{s)}$ , respectively. The lower wall of the cylinder constitutes one of the electrodes and the central area of the upper wall is the second electrode, thus generating axially symmetric electric current lines. The working fluid's upper level touches the upper electrode's lower extreme leaving a free surface ring exposed to the atmosphere to allow hydrogen bubbles to escape when electrolysis occurs. Two Neodymium magnets are placed above and below the cell. The arrangement results in an approximately uniform magnetic field distribution in the vertical direction oriented upwards with an average magnitude of  $B_0 = 0.08 \text{ T}$ . An axial electric current in the range of  $4 \text{ mA} \leq I \leq 6 \text{ mA}$  is applied to the working fluid through the electrodes. A shroud made of a larger diameter transparent cylindrical wall was added for optical coupling (see Fig. 1). To record the poloidal velocity field, a two-dimensional Particle Image Velocimetry (PIV) system is applied to a laser sheet illuminated vertical plane passing through the axis of symmetry of the cylinder. The flow images were captured using a Nikon D300s camera at a resolution of  $1280 \times 720$  pixels (px), which was mounted on a tripod at approximately 30 cm from the cavity, fitted with AF-S VR Micro-Nikkor 105 mm f/2.8G IF-ED lens facing parallel to the device. The fluid was seeded with Dantec Dynamics S-HGS-10 particles, which are silver-coated hollow glass spheres with a mean particle diameter of  $10 \mu\text{m}$ . Using as characteristic length  $\sqrt{\sigma/\mu}$  the height of the cylindrical cavity,  $L = 0.03 \text{ m}$ , the Hartmann number is  $\text{Ha} = B_0 L \sqrt{\sigma/\mu} = 0.17$ .

## 2. Experimental observations.

As explained in Section 1, in the experimental configuration considered the magnetic field is approximately uniform in the  $z$ -direction and the electric current density is mostly vertical except in the region near the upper electrode, where the current lines are slightly bent towards the axis of symmetry. Given that the magnetic field and the electric current are approximately parallel in most of the cavity, a negligible Lorentz force is produced. Only in the vicinity of the upper horizontal boundary region, the force is noticeable.

*Lorentz force induced flow in a cylindrical container*

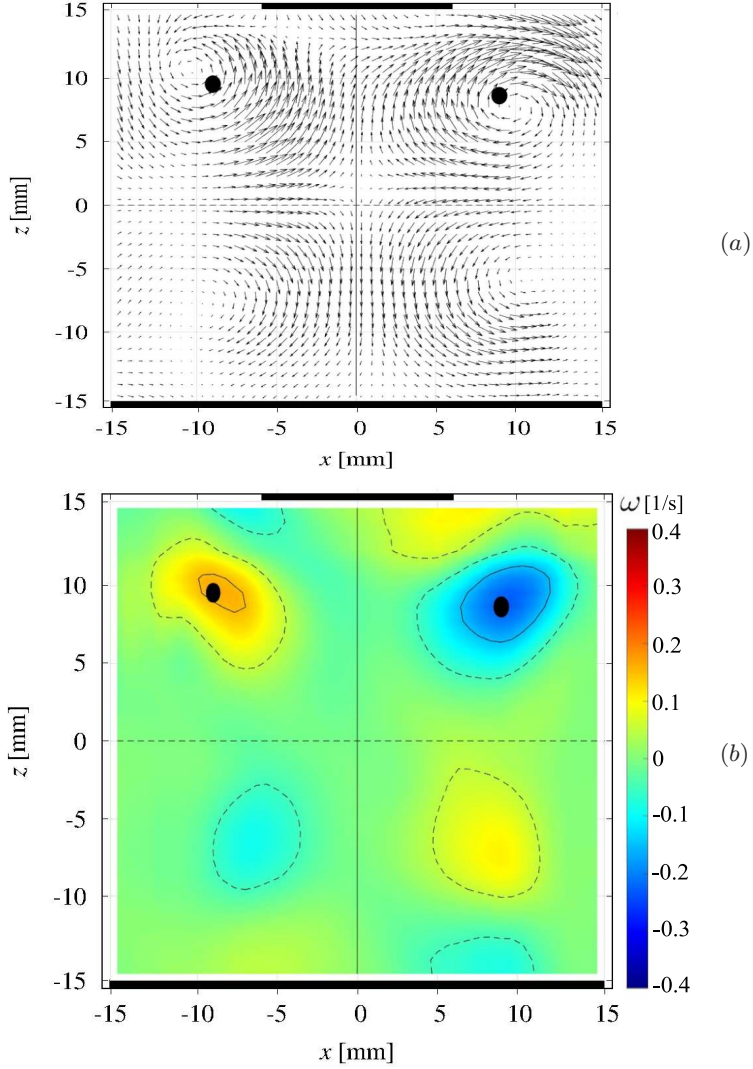


*Fig. 2.* (a) Average velocity field projection observed over an interval of 275 s. (b) Normal vorticity component in the observed vertical plane. Average magnetic field 0.08 T, electric current +4 mA. Black dots indicate monitor positions.

Close to the right corner in the figure the force points into the plane and away from the plane in the region close to the left corner. Therefore, the force drives a counterclockwise rotating motion around the axis of symmetry with a dominant azimuthal velocity which, in turn, produces a secondary poloidal flow.

Experimental observations were made when applying electric currents of 4, 5, and 6 mA. Although the forces driving the flow are time-independent, the motion displays a non-steady behavior. Before we address the properties of the time-dependent motion, to simplify the description, we shall discuss the details of the average features of the poloidal flow taken over an interval of 275 s. Fig. 2 shows the average velocity field

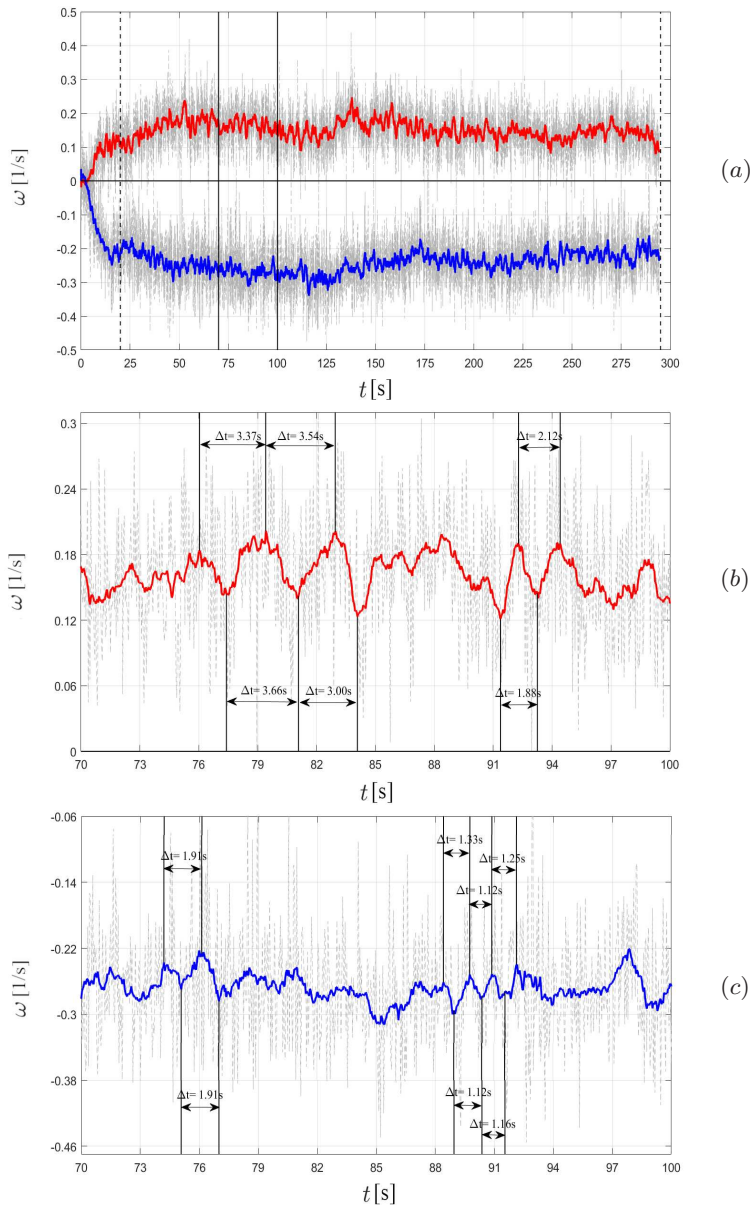


*Fig. 3.* Time-dependent vorticity component normal to the observed vertical plane sampled at fixed positions. Upper panel (a): The light gray traces are raw data and thick red and blue traces are running averages with a 0.41 s window. Monitor points, red trace  $x, z = -9.1, 7.2$  mm; blue trace  $x, z = 9.1, 8.1$  mm. Lower panels (b) and (c): Amplification of the upper plot to show samples of approximately periodic fluctuations. Average magnetic field 0.08 T, electric current +4 mA.

projection on a vertical plane passing through the axis of symmetry of the cylinder and the corresponding normal component of the vorticity obtained from PIV measurements.

The upper part of the field features ascending fluid near the central line and des-

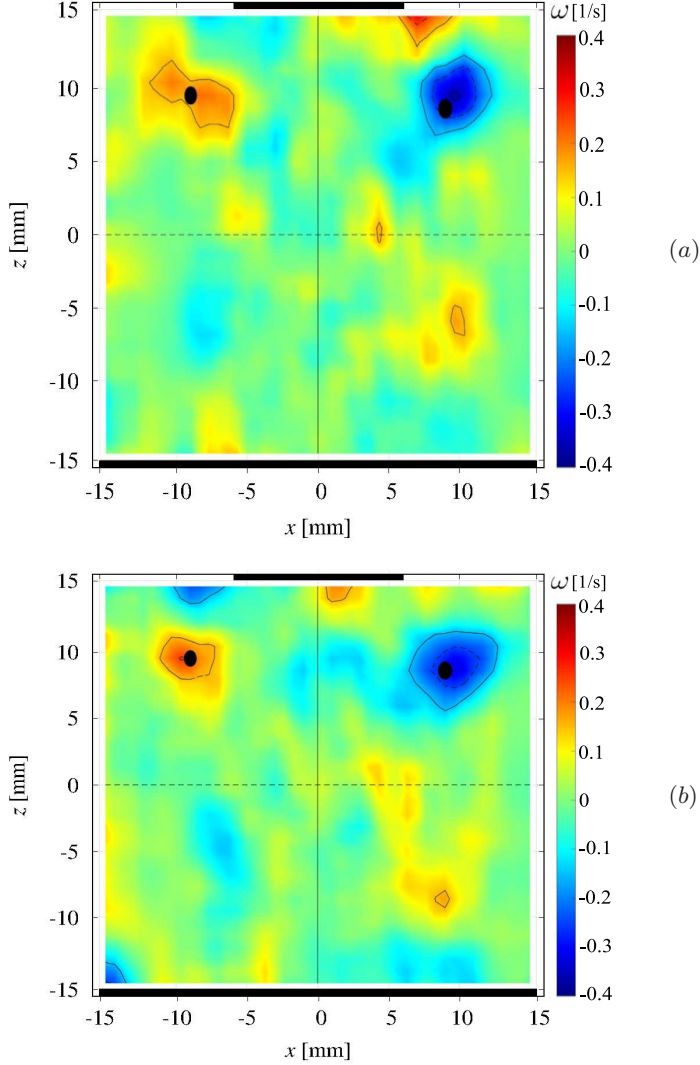


*Fig. 4.* Vorticity field in the vertical plane for sample times. (a) Local minimum,  $t = 91.4$  s and (b) local maximum  $t = 92.3$  s. Black dots are the monitor positions for the traces shown in Fig. 3.

ending close to the vertical walls. Mass conservation promotes the formation of rotating structures that constitute the vortices seen on the left side of Fig. 2. A similar velocity field with vectors reflected with respect to the mid-horizontal line forms in the lower half of the cavity, but the upper pair of vortices are about a factor of two more intense than the lower ones. The two pairs of counter-rotating vortices are located approximately symmetrically with respect to the central vertical axis, and the swirl is such that the motion near the axis of symmetry points towards the electrodes. To explore the time-dependent behavior of the system, we show with light gray traces in Fig. 3 the history of the normal vorticity component at two positions,  $x = -9.1$  mm,  $z = 7.2$  mm and  $x = 9.1$  mm,  $z = 8.1$  mm with an electric current of +4 mA. The red (positive) and

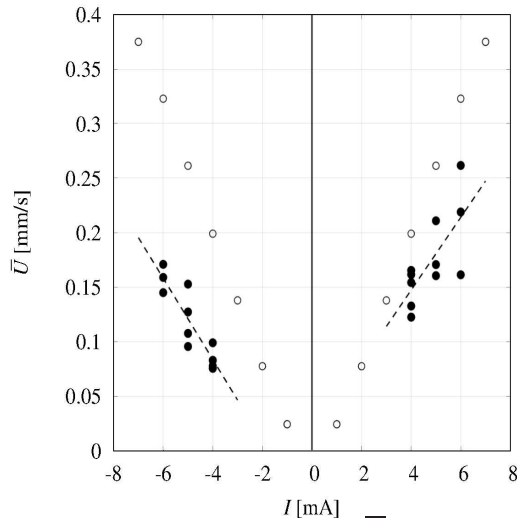


*Fig. 5.* Time and space average velocity magnitude  $\bar{U}$  in the observed plane as a function of the externally imposed electric current ( $I$ ). The solid dots represent individual experimental realizations. The empty dots correspond to velocity averages calculated with the steady state model described in Section 3.

blue (negative) traces are running averages with a time interval window of 0.41 s of the original observations. Irregular fluctuations with amplitudes of approximately  $0.1 \text{ s}^{-1}$  are superimposed to a nearly constant vorticity of  $\omega = +0.15$  and  $-0.24 \text{ s}^{-1}$  at the two monitoring points. In this particular observation positions, the vortices are not symmetrical. Fourier analysis indicates that although many modes are present, the smaller dominant frequencies for the positive and negative traces can be identified and are, respectively,  $f_1^+, f_2^+, f_3^+ = 0.14, 0.29, 0.43 \text{ s}^{-1}$  and  $f_1^-, f_2^-, f_3^- = 0.12, 0.26, 0.33 \text{ s}^{-1}$ . In both cases,  $f_2/f_1 \sim 2$  and  $f_3/f_1 \sim 3$ . Figs. 3*b,c* display amplifications of the traces to show the presence of bursts of approximately regular oscillations. Also, note that the relatively large amplitude in the oscillation of one trace does not necessarily correspond to similar oscillations in the other. This implies independent, local pulsations of the vortices. To illustrate the physical origin of the fluctuations in the vorticity traces, the vorticity spatial distributions are shown in Fig. 4 for  $t = 91.4$  and  $92.3$  s, which correspond, respectively, to a local minimum and maximum of the red trace of Fig. 3. At  $t = 91.4$  s, the positive vorticity features an elongated (orange-red region), whereas for  $t = 92.3$  s, the vorticity distribution is a more intense nearly circular distribution. The amplitude of the vorticity fluctuations is a weak function of the electric current in the range explored, in all cases being about  $0.1 \text{ s}^{-1}$ . The deflection of the traces indicates the presence of positive and negative vortical structures suggested by the gray loops. Similar structures with smaller vorticity form in the lower half of the cell.

To detect the intensity of the motion generated by the poloidal flow, we calculated the average velocity magnitude taken on the observed plane, over the entire observation window (time and space-average  $\bar{U}$ ), that is

$$\bar{U} = \frac{1}{t_f - t_0} \int_{t_0}^{t_f} \sqrt{U_x^2 + U_z^2} dt. \quad (1)$$

In the previous equation,  $t_0$  and  $t_f$  are the observation window's initial and final times, respectively. The symbols  $U_x$  and  $U_y$  are the space-averages of the poloidal velocity in the observed plane. In Fig. 5, the experimental average velocity is shown with solid dots for at least three experimental realizations of each electric current explored. Average velocities corresponding to positive currents are larger and show more dispersion than their negative current counterparts. Linear trends are suggested for positive and negative electric currents, with a larger slope for the positive cases. The asymmetry of the experimental points relative to the current direction could result from an uncontrolled deviation from axial symmetry. The average velocity  $\bar{U}$  calculated with a steady-state numerical model described in the next section is shown in the same figure with open dots. Linear dependences on the electric currents and symmetric trends are obtained for positive and negative currents. For positive currents, the calculations overestimate the observations by 25% to 40%, while for negative currents, the overestimation is larger.

### 3. Analysis.

Given the shape of the container and the relative position of the magnets and electrodes, the main velocity generated by the Lorentz force is in or out of the illuminated plane in the upper part of the cylinder. The experimental velocity field shown in Fig. 2 indicates that although no imposed force is present in the vertical plane, a substantial motion in this plane organized in two counter-rotating vortices is observed. While this is not inconsistent with the expected azimuthal motion generated by the Lorentz force, elaboration to fully reconstruct the three-dimensional flow is required. One would be tempted to explain the motion in the vertical plane in terms of the Bödewadt flow that consists of a swirling flow in a fluid limited by a stationary rigid plate perpendicular to the rotation vector [4]. The centrifugal force sets up a radial pressure gradient in the opposite direction establishing the dynamic equilibrium. In the boundary layer near the plate, the rotating velocity is reduced, the radial pressure gradient drives a radial motion towards the axis of rotation, where the pressure is low. In turn, the converging radial motion generates a jet away from the plate and into the rotating flow. A dipole-type flow ensues due to mass conservation. The expression  $\delta = 4(\nu/\Omega)^{1/2}$  estimates the scale of the boundary layer thickness. There are two difficulties in interpreting our observations as the Bödewadt's flow. First, in our experiment,  $\nu = 0.9 \times 10^{-6} \text{ m}^2/\text{s}$ ,  $\Omega \sim 1.6 \times 10^{-2} \text{ 1/s}$  and  $\delta = 3 \times 10^{-2} \text{ m}$  and, therefore, the boundary layer fills the whole cavity. Second, the flow observed runs in the opposite direction as predicted by the Bödewadt flow limited by an infinite rigid wall. In our setup, the flow is indeed limited by the solid electrode in the region close to the axis of symmetry,  $r < 0.015 \text{ m}$  and then by a free surface in  $0.015 \text{ m} < r < 0.03 \text{ m}$ . Under this complex boundary it is unlikely that the simple Bödewadt theory can be applied.

To describe the full three-dimensional pattern of the flow, the velocity and pressure fields were numerically calculated to analyze the dynamics further using COMSOL Multiphysics with the Lorentz force included as a source in the momentum equation. Although the flow is time-dependent, a steady state is assumed in the numerical model, and the results are interpreted to correspond to the average flow described in Fig. 2. The velocity and pressure fields for an electric current of +4 mA are shown in Figs. 6a,b.

As observed in Fig. 6a, the motion is composed by vortices with the fluid ascending near the axis of symmetry, coinciding with the observed velocity and vorticity fields of Fig. 2. Inspection of the pressure field shown in Fig. 6b indicates that the pressure is largest near the free surface ring; as a consequence, pressure gradients form in the core of the fluid. Simplifying the picture, we identify a horizontal gradient that promotes the

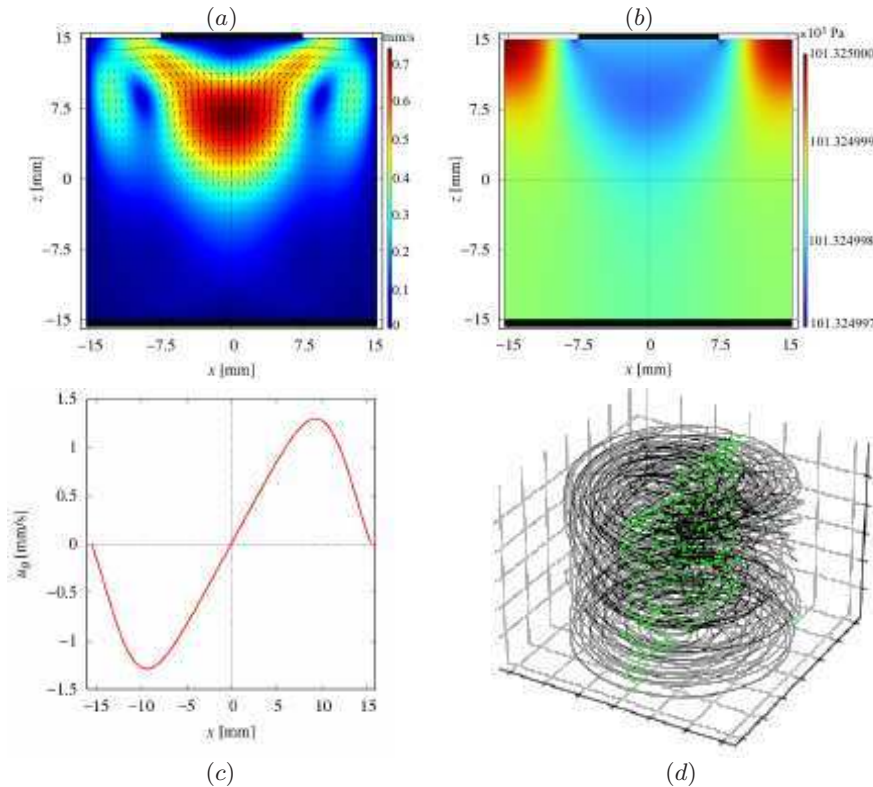


*Fig. 6.* Numerical flow simulation with an upward +4 mA electric current. (a) Projection of the velocity field in the  $(x, z)$ -plane. (b) Pressure field in the  $(x, z)$ -plane. (c) Azimuthal component  $u_\theta$  velocity profile for  $z = 8$  mm. (d) Lagrangian orbit. Initial point  $x_0 = -0.8$  mm,  $y_0 = 0.5$  mm,  $z_0 = -14.9$  mm. Green points indicate the intercepts of the orbit with the  $x = 0$  plane.

converging flow towards the central line, akin to the Bödenwadt's effect and crucially, a vertical flow that forces a descending motion near the lateral wall. Mass conservation organizes a flow return of the ascending fluid near the symmetry line. This structure dominates the poloidal flow observed in the experiments. The calculated pressure distribution (Fig. 6b) is consistent with the interpretation given above.

Fig. 6c shows the profile of the azimuthal velocity component as a function of the horizontal coordinate along the diameter of the cylindrical cavity at  $z = 8$  mm. The numerically calculated streamlines are shown in Fig. 6d. The full orbit structure is complex, but a detailed analysis of intercepts of the orbit with the plane  $x = 0$  shown as green dots reveals that ordered structures can be identified in the regions close to the center of the vortices. The orbit forms nested loops with those closer to the common center. In the ordered segments it is reasonable to suggest that the orbit is embedded on the surface of tori. In the central loop, the orbit takes approximately four poloidal turns before completing a toroidal cycle. In the next smaller loop, the orbit takes approximately six poloidal turns. The actual experimental traces are unlikely to coincide in detail with those obtained by steady-state numerical integrations. Specifically, a more accurate calculation of the velocity field and Lagrangian tracking to build the tracer's paths is required. This constitutes the subject of an ongoing study.

**Concluding remarks.**

We have analyzed experimentally and numerically the electrolyte flow in a cylindrical cavity driven by a Lorentz force produced by the interaction of a mostly axial electric current and an approximately uniform vertical magnetic field. The curvature of the current paths near the upper electrode generates an azimuthal Lorentz force that produces a swirling flow. This, in turn, gives rise to a secondary poloidal flow which was analysed through PIV. Although physical conditions in the explored flow are very different from those present in liquid metal EVF, flow patterns exhibit some interesting similarities. In particular, in liquid metal flows, secondary poloidal flows were observed as a consequence of the interaction of the curved electric current lines with their induced magnetic field [3], as well as as a result of a counter-rotating swirling flow in a symmetrical electrode configuration with an applied axial magnetic field [5].

**Acknowledgments.**

This work was supported by UNAM-DGAPA-PAPIIT under project IN107722. M.D. Marín-Núñez and D.R. Domínguez-Lozoya thank, respectively, PhD and postdoctoral grants from CONAHCYT, Mexico. We are grateful to the anonymous referee for valuable suggestions that have improved the manuscript.

**References**

- [1] D. KELLEY AND T. WEIER. Fluid Mechanics of Liquid Metal Batteries. *Applied Mechanics Reviews*, (2018).
- [2] V. BOJAREVICS, Y. FREIBERGS, E.I. SHILOVA, AND E.V. SHCHERBININ. *Electrically Induced Vortical Flows*, vol. 53 (Kluwer Academic Publishers, 1989).
- [3] I. KOLESNICHENKO, *et al.* Evolution of a strong electrovortex flow in a cylindrical cell. *Physical Review Fluids*, vol. 5 (2020), no. 12, p. 123703.
- [4] P.A. DAVIDSON. *An introduction to magneto-hydrodynamics* (Cambridge University Press, 2017).
- [5] S. BÉNARD, W. HERREMAN, J. GUERMOND, AND C. NORE. Numerical simulations of swirling electrovortex flows in cylinders. *J. Fluid Mech.*, vol. 950 (2022), p. A28.

Received 09.12.2024